Probing the catalytically active species in POM-catalyzed DNA-model Hydrolysis

Frederico F. Martins,[a] Dr. Ángel Sánchez-González,[a] Jose Lanuza, [b,c] Dr. Haralampos N. Miras,*[d] Prof. Xabier Lopez,[b,c] Dr. Nuno A. Bandeira*[a] and Dr. Adrià Gil*[a,e]

[a] MSc. F, F, Martins; Dr. A, Sánchez-González; Dr. N, A, Bandeira; Dr. A, Gil
BioISI – Biosystems and Integrative Sciences Institute, Departamento de Química e Bioquímica, Faculdade de Ciências
Universidade de Lisboa
8.5.53 C8 bdg, Campo Grande, 1749-016 Lisboa, Portugal
E-mail: a.gil@nanogune.eu
agmestres@fc.ul.pt
nuno.bandeira@ciencias.ulisboa.pt

[b] MSc. J, Lanuza; Prof. X. Lopez
Polimero eta Material Aurreratuak: Fisika, Kimika eta Teknologia Saila, Kimika Fakultatea, Euskal Herriko Unibertsitatea (UPV/EHU), Paseo Manuel de Lardizabal 3, 20018 Donostia-San Sebastián, Spain

[c] MSc. J, Lanuza; Prof. X. Lopez
Donostia International Physics Center (DIPC), Paseo Manuel de Lardizabal 4, 20018 Donostia-San Sebastián, Spain

[d] Dr. H, N, Miras
School of Chemistry
University of Glasgow
Joseph Black Building, Glasgow, G12 8QQ, UK
Email: Charalampos.Moiras@glasgow.ac.uk

[e] Dr. A. Gil
CIC nanoGUNE BRTA
Tolosa Hiribidea 76, E-20018, Donostia - San Sebastian, Euskadi, Spain

Supporting information for this article is given via a link at the end of the document.

Abstract: Phosphoester hydrolysis is an important chemical step in DNA repair. One archetypal molecular model of phosphoesters is para-nitrophenylphosphate (pNPP). It has been shown previously that the presence of molecular metal oxide $[Mo_7O_{24}]^{6-}$ may catalyse the hydrolysis of pNPP through the partial decomposition of polyoxomolybdate framework resulting in a $[(PO_4)_2Mo_5O_{15}]^{6-}$ product. Real-time monitoring of the catalytic system using electrospray ionisation mass spectrometry (ESI-MS) provided a glance into the species present in the reaction mixture. Following up on the obtained spectrometric data, Density Functional Theory (DFT) calculations were carried out to characterise the hypothetical intermediate $[Mo_5O_{15}(pNPP)_2(H_2O)_6]^{6-}$ that would be required to form under the hypothesised transformation. Surprisingly, our results point to the dimeric $[Mo_2O_8]^{4-}$ anion resulting from the decomposition of $[Mo_7O_{24}]^{6-}$ as the active catalytic species involved in the hydrolysis of pNPP rather than the originally assumed $\{Mo_5O_{15}\}$ skeleton. A similar study was carried out involving the same species but substituting Mo by W. The mechanism involving W species showed a higher barrier and less stable products in agreement with the non-catalytic effect found in experimental results.

Introduction

Polyoxometalates (POMs) are negatively charged metal oxide clusters known since 1826[1] (see Figure 1). Classical POM archetypes are mainly formed from d^0 metal oxides made of V, Mo or W which can undergo condensation reactions at acidic pH with subsequent loss of H_2O.[2] Nevertheless, during the last years we can find examples of similar polyanionic nanostructures containing elements for the f [3-6] and p groups.[7,8]

During the last years, the applications of this family of compounds have been explored intensively and found their way in various fields such as the decontamination of water,[9] flash memory devices,[10] qubits,[11] water splitting[12] as well as in biomedical research exploring their function as antiviral or antitumoral drugs.[13-15] However, biomedical studies were still scarce in the latter case in the '90s as discussed in the review of Rhule et al.[13] It was during the early-mid 2000 when systematic studies on the application of POMs to cancer treatment increased exponentially.[14,16-20] Additionally, recent advances in the use of POMs for medical applications, their antitumor activity[21] and their potential use to fight against bacterial antibiotic resistance[22,23] have been reviewed by Bijelic et al.[21,22] and Kortz et. al.[23]

According to Bijelic et al.[21,22] the proposed modes of antitumoral action of POMs involves a high number of biological targets: 1) Activation of cell death pathways, 2) Inhibition of angiogenesis, 3) Interaction with proteins or 4) DNA interaction among other mechanisms. On the other hand, the proposed mechanisms of action against bacteria involve: a) inhibition of both PBP2a and β–lactamases by POMs, b) POMs target P-type ATPases, c) impairment of the bacterial electron-transport chain (respiratory system) by POMs, d) POM-mediated increase of the reactive oxygen species level via oxidation, e) interaction of POMs with important membrane-anchored proteins and enzymes, f) the disruption of the bacterial cytoskeleton dynamics by POM-interactions with cytoskeletal elements, g) disruption of

the bacterial cell wall leading to leakage of intracellular substances or h) interaction with cytoplasmic elements or proteins that are anion-sensitive like nucleic acid-binding proteins. As discussed earlier, one of the processes described in the reviews of Bijelic et al.[21,22] is the interaction of POMs with DNA to promote its phosphoester hydrolysis as artificial phosphoesterases. The study of this step is the focus of this work.

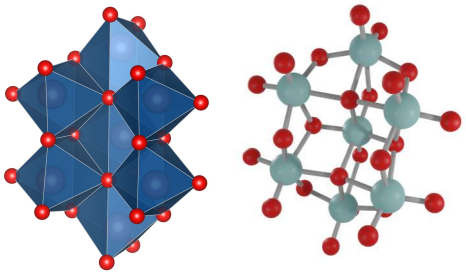

Figure 1. Polyhedral (left) and ball & stick (right) structures of the $[Mo_7O_{24}]^{6-}$ system studied in this work.

The phosphoester bond is produced when any hydroxyl group of the phosphoric acid react with hydroxyl groups of neighbouring molecules to form an ester bond. In the case of DNA, two bonds are formed from two hydroxyl groups of the phosphoric acid with the deoxyribose sugars forming the DNA strand to form the phosphodiester bond (see **Scheme 1**). These types of bonds are extremely stable and therefore play a very important role to maintain the integrity of the genetic code and the proper function of proteins. Consequently, nature has devised these links to maintain the connectivity of nucleosides in DNA, with remarkable kinetic stability: the half-life for hydrolysis of phosphoester bonds in DNA at neutral pH and 298 K is estimated to be 130 kyears.[24] This resistance to hydrolysis is mainly due to the repulsion between the negatively charged backbone and the potential nucleophiles which are also negatively charged, consequently, an important Coulombic repulsion has to be surmounted in order to produce the hydrolysis, leading to high activation energy during the course of the phosphoester hydrolysis.[25]

This stability of the phosphoester can be overcome through a family of enzymes known as phosphoesterases. These catalysts play an important role in repairing DNA sequences[26] allowing the rate increase of the phosphoester bond hydrolysis. Thus, the development of artificial catalysts which promote the phosphoester bond hydrolysis in reasonable time scales is an important research topic that has been explored extensively in the last 15 years.[25,27-53] These artificial catalysts include Cu(II),[54] Zn(II),[55] Lanthanide(III),[56-58] Mo(V/VI) complexes[25,35,36] and/or POM clusters.[27-32,39-41,43,45-47]

Particularly surprising is the catalysis of the phosphoester bond by polyoxoanions since an also negatively charged phosphate group will need to coordinate to them in order to facilitate a nucleophilic attack by water. A deeper understanding and rationalization of the catalytic mechanism involving POMs and chemical species with phosphoester bonds is inherently highly challenging.

In previous studies, Parac-Vogt et al.[41,46] attempted to tap into the mechanistic action of $[Mo_7O_{24}]^{6-}$ ({Mo_7}) in phosphoester hydrolysis employing model substrates and using several experimental techniques.

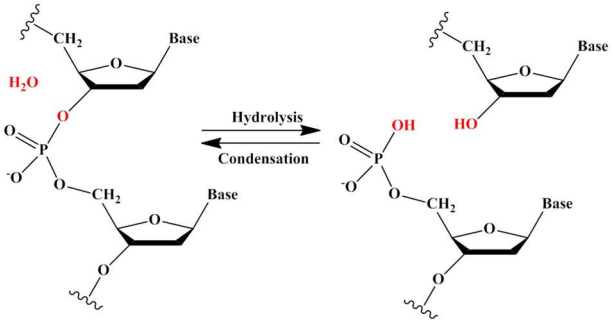

Scheme 1. Phosphodiester hydrolysis in DNA.

Their work consisted of the hydrolysis of *para*-nitrophenylphosphate (hereafter named pNPP) in the presence of a {Mo_7} solution.[27-30] The pNPP molecule is a typical model substrate of the phosphoester bond in DNA.

In their account, Parac-Vogt et al.[27] clearly found that the hydrolysis was activated in the presence of {Mo_7} and subsequently proposed a set of transformation steps based on their findings, notably ^{31}P and ^{1}H and DOSY NMR, UV-Vis and RAMAN spectroscopies. It was found that during the course of this reaction a side product $[Mo_5O_{15}(PO_4)_2]^{6-}$ ({Mo_5-PO_4}) anion was formed (see **Figure 2**) previously identified by Fischer and others.[64]

Based on this evidence the authors proposed two transformative steps () conducive to a hypothetical intermediate species $[(pNPP)_2Mo_5O_{21}]^{4-}$ ({Mo_5-pNPP}) and $[(pNPP)_2Mo_{12}O_{36}(H_2O)_6]^{4-}$ (Intermediates **A** and **B** on the original paper).

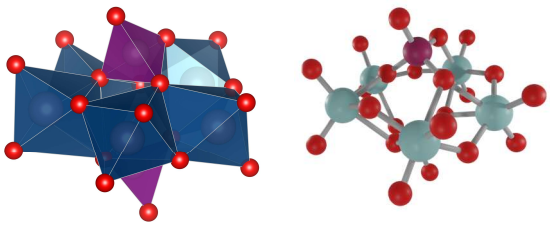

Figure 2. Polyhedral (left) and ball & stick (right) representation of the $[Mo_5O_{15}(PO_4)_2]^{6-}$ anion.

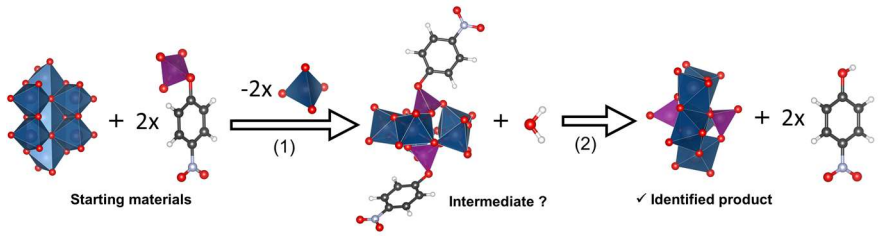

(1)+(2): $[Mo_7O_{24}]^{6-}$ +2$[NO_2PhOPO_3]^{2-}$ +H_2O→$[(PO_4)_2Mo_5O_{15}]^{6-}$ + 2(NO_2PhOH) + 2$[MoO_4]^{2-}$

Figure 3. Proposed chemical reactions (ref. 28) of the hydrolysis of pNPP catalysed by heptamolybdate. The phosphate groups are represented by purple hatched polyhedra.

One aspect is particularly striking in the previously reported work: The disparity in geometries between the {Mo_5-PO_4} product and the {Mo_7} starting material. There is no simple obvious route from the latter to the former other than (1) the complete disassembly and subsequent re-assembly into {Mo_5-PO_4} or (2) a significant structural rearrangement within the {Mo_5} framework.

The primal goal in this work is to unveil some of these obscure aspects in this particular reaction step. As such it was decided to revisit this work employing both experimental (ESI-MS) and computational approaches (DFT).

Herein we start out by analysing the {Mo_7}+pNPP reaction mixture using ESI-MS which can provide us with potential intermediate candidates and using these as a starting point to carry out a reaction path analysis *in silico* of the hydrolysis process.

Our new results highlight the fact that the $[Mo_5O_{15}]^0$ ({Mo_5}, species which is the predecessor of the identified {Mo_5-PO_4}) is not the catalytically active species. We propose an alternative sequence of transformations where the original {Mo_7} reactant dissociates into two moieties: one dinuclear $[Mo_2O_8H_4]$ ({Mo_2}), and a pentanuclear {Mo_5} species. The former species is the agent that catalyses the hydrolysis whereas the latter will capture the resulting phosphate.

Additionally, the generation of the $[Mo_2O_8H_4]$ and $[Mo_5O_{15}]$ species was corroborated by mass spectrometry experiments. Finally, the effect of solvent was considered not only with the dielectric continuum approach but also with a minimal number of explicit H_2O molecules which provide a more accurate portrayal of the energy barrier corresponding to the pentacoordinate transition state.

Results and Discussion

ESI-MS spectrometry

In an effort to characterize further the clusters in solution and identify unambiguously the structural integrity and composition of the species formed during the course of the reaction, we employed high-resolution electrospray ionization mass spectrometry (ESI-MS) and monitored in real time the reaction mixture.[59] The ESI-MS studies were performed in water/methanol (20:80). The speciation and fragment rearrangements were investigated as follows.

Sodium heptamolybdate, $Na_6[Mo_7O_{24}]$ and pNPP were dissolved in aqueous solution and stirred at 50°C for approximately 30 h. Aliquots were removed at noted time intervals throughout the reaction, diluted with methanol, and analysed using ESI-MS (the parameters for which were consistent throughout all runs). The first spectrum was recorded upon mixing the starting materials (t = 0) and after the reaction mixture had been stirred at 50°C for 1, 3 and 30 hours, respectively. In both cases, the observation of the higher intensity set of distribution envelopes is due to the existence of the heptanuclear moiety, resulting from the combination of protons, counterions and solvent molecules. Additionally, transition metal clusters are generally susceptible to redox processes. The observed change of the oxidation state of the metal centres is due to the ionization and consecutive ion-transfer process of the charged species and has been observed previously on numerous occasions.[60-62] In this case, the region of higher m/z values is populated by a series of distribution envelopes assigned to –1 charged species and can be assigned to the {Mo_7} intact cluster (**Figure 4**, **Table 1**) with the corresponding distribution envelopes centred at c.a. 1103.27, 1225.25 and 1249.24 m/z. The intensity of the envelopes corresponding to the intact {Mo_7} cluster can be detected clearly the first 3 hours of the reaction while their relevant intensity gradually decreases to the point where cannot be detected any more (t = 30 h). As expected, the peak centred at 217.90 m/z can be assigned to the singly charged organic molecule of $[NO_2C_6H_4PO_4H]^-$.

Interestingly, the lower region of m/z values (*ca*. 300 – 1100) revealed additional information regarding the building block units that can be generated in situ during the course of the catalytic reaction. The distribution envelopes centred at 304.77, 448.66, 470.64 and 510.72 m/z values have been identified as trimeric {Mo_3} units associated with different number of counterions and solvent molecules while the envelope at 614.52 m/z could be assigned to the tetrameric molybdenum moiety, $\{Mo_4O_{13}Na\}^-$. Interestingly, two envelopes centred at 654.72 and 670.61 m/z values have been identified as the {Mo_2} dimeric pNPP adducts revealing the ability to the lower nuclearity species to form hybrid complexes with the organic moiety. The higher m/z region (800 – 1000 m/z) revealed the formation of penta-molybdodiphosphate-based, $[Mo_5O_{15}(PO_4)_2]^{6-}$, derivatives which typically form in mildly acidic solutions containing molybdate and phosphate ions.[63] However, it has been reported that the $[Mo_5O_{15}(PO_4)_2]^{6-}$ anion does not induce the cleavage of the phosphoester bond in pNPP, even after prolonged reaction times[28] which is an indication that the species forms in situ due to the presence of free PO_4^{3-} anions originating from the cleavage of phosphate groups. Overall, the various species identified during the first hours of the reaction (t = 0 – 3), degrade over time and only dimeric and trimeric species can be identified after 30 hrs. These observations collectively increase our understanding of the rearrangement processes taking place in the reaction solution.

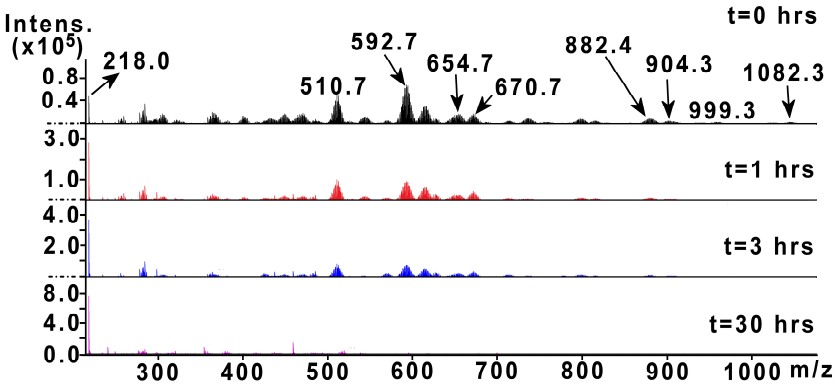

Figure 4. Negative mode electrospray ionisation mass spectrum (ESI-MS) of the reaction mixture in H_2O:CH_3OH (20:80).

In summary, several peaks were observed for {Mo_5} related species (m/z= 882.40 to 999.35) that incorporate either one or two phosphate groups. These species have been identified and reported previously in the literature.[64] Interestingly, none of the identified species corresponds to an adduct of {Mo_7} (1103.27 < m/z < 1249.24) or {Mo_5} type fragment with the pNPP anion as was hypothesised in the initial studies.[28]

Table 1. Representation of the experimentally identified and simulated m/z values of distribution envelopes corresponding to the species in the reaction mixture.

Exp.	Theor.	Charge	Chemical formula
218.00	217.98	-1	$[NO_2C_6H_4PO_4H]^-$
304.77	304.74	-1	$[Mo_2O_7H]^-$
448.66	448.70	-1	$[Mo_3O_{10}H]^-$
470.64	470.65	-1	$[Mo_3O_{10}Na]^-$
510.72	510.70	-1	$[Mo^{IV}Mo^{V}_2O_9Na(H_2O)_3H_2]^-$
592.65	592.75	-1	$[Mo_3O_{15}(H_2O)_3H_{11}]^-$
614.52	614.54	-1	$[Mo_4O_{13}Na]^-$
654.72	654.61	-1	$[Mo^{IV}Mo^{V}O_7(NO_2C_6H_4PO_4)(Na)_5(H_2O)H]^-$
670.61	670.71	-1	$[Mo^{V}Mo^{VI}O_8(NO_2C_6H_4PO_4)(Na)_5(H_2O)H]^-$
882.40	882.31	-1	$[Mo_5P_2O_{21}NaH_5]^-$
904.29	904.39	-1	$[Mo^{IV}Mo^{V}_4P_2O_{21}NaH_4]^-$
999.35	999.36	-1	$[Mo^{V}_5P_2O_{23}Na_3(H_2O)H_3]^-$
1017.47	1017.37	-1	$[Mo^{V}_5P_2O_{23}Na_3(H_2O)_2H_3]^-$
1046.22	1046.35	-1	$[Mo^{IV}Mo^{V}_4P_2O_{21}Na_5(H_2O)_3]^-$
1082.30	1082.37	-1	$[Mo^{IV}Mo^{V}_4P_2O_{21}Na_5(H_2O)_5]^-$
1103.27	1103.34	-1	$[Mo^{V}_3Mo^{VI}_4O_{24}Na(H_2O)H_7]^-$
1225.25	1225.20	-1	$[Mo^{V}Mo^{VI}_6O_{24}Na_5(H_2O)_3H]^-$
1249.24	1249.20	-1	$[Mo^{V}_3Mo^{VI}_4O_{24}Na_6(H_2O)_3H_2]^-$

Computational studies

Based on the evidence provided by the ESI-MS studies that a direct acid-base adduct of pNPP with $[Mo_7O_{24}]^{6-}$ is unlikely to take place, we proceeded initially to quantify the non-catalysed organic hydrolysis step in a computational study and used it as a reference point for the catalytic steps. Two kinds of mechanisms are traditionally proposed for the non-catalysed reaction. That is, 1) the **substrate-assisted** mechanism in which the phosphate acts as a proton acceptor of an incoming water molecule and 2) the **solvent-assisted** mechanism in which there is a straightforward nucleophilic substitution of nitro-phenolate with water. In prior studies[65] the most appropriate description of these two mechanisms entailed the use of explicit water molecules. For this reason, it was decided to include four in all the models as the best compromise between expediency and accuracy. The energy profiles of these mechanisms with the inactivated pNPP molecule are depicted in **Figure 5**. The values of $\Delta G^{\ddagger}$=+29.8 kcal mol^{-1} for the substrate assisted and $\Delta G^{\ddagger}$=+21.4 kcal mol^{-1} for the solvent assisted pathways are in line with previous computational studies.[65]

As the product that is detected in the Parac-Vogt studies[28] is $[Mo_5P_2O_{23}]^{6-}$ the natural step would be to reconstruct this phosphate templating reaction by performing the hydrolysis of grafted pNPP to reach this product. A reasonable starting species for this would be $[Mo_5O_{15}(pNPP)_2]^{4-}$. The production of the pentacoordinate phosphorus intermediate has an activation barrier that is 11 kcal mol^{-1} higher than the activation barrier of the uncatalysed substrate assisted reaction and 19 kcal mol^{-1} higher than the barrier for the solvent assisted pathway (see **Figure 6**). The POM activated pathways involve an O-H bond cleavage from an incoming water molecule to one oxygen of the POM structure, resulting in a substrate-assisted type mechanism. For the $[Mo_5O_{15}(pNPP)_2]^{4-}$ the transition state leads to an intermediate λ^5-phosphate(V) containing structure that is a confirmed local minimum in energy. Subsequent searches for a solvent assisted mechanism with this {Mo_5} activator proved unsuccessful. This is probably due to the latent Brønsted acidity in polyoxoanions which makes proton transfers ubiquitous. Clearly, these results are inconsistent with the proposal set out in ref. 28 (**Figure 3**), i.e. that an {Mo_5} species is directly responsible for the higher rate of hydrolysis. The only adduct with pNPP that is observed in the ESI-MS study given above is with a dinuclear entity ($[Mo_2O_8(NO_2C_6H_4PO_4)(Na)_5(H_2O)H]^-$). In the light of this observation it was decided to explore the catalytic ability of a dinuclear model with a reasonable formulation such as

$[Mo_2O_4(OH)_4(pNPP)]^{2-}$ ($\{Mo_2\}$) i.e. two edge-sharing octahedra capped with equatorial hydroxy groups, herein represented in **Figure 7**. Four explicit water molecules were included in this model to make it comparable to the organic reaction (**Figure 5**). Proton isomers of this species were pre-screened, and their energies are presented in the supporting information section.

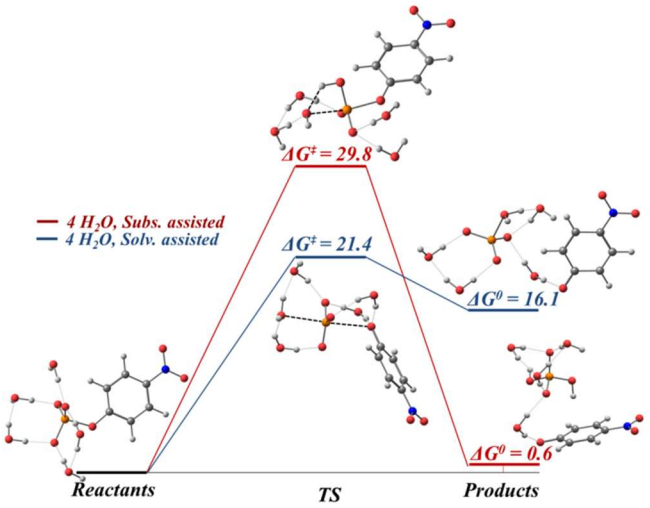

Figure 5. Reaction schemes for pNPP hydrolysis with no catalyst. Gibbs free energies in kcal mol^{-1}.

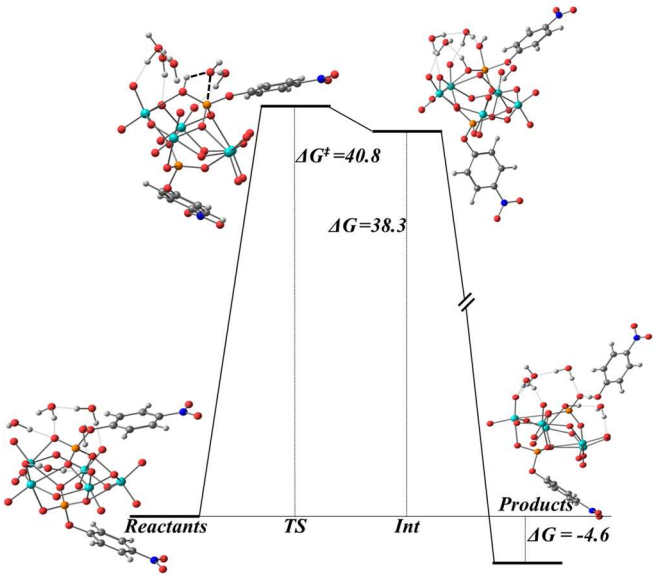

Figure 6. Reaction scheme for pNPP hydrolysis $[Mo_5O_{15}(pNPP)_2(H_2O)_6]^{6-}$. Gibbs free energies in kcal mol^{-1}.

The results of the hydrolysed activation with $\{Mo_2\}$ are presented in Figure 8 along with the activation barrier height. When comparing these values to the non-catalysed pathways shown in Figure 5 a more favourable kinetics scenario is observed. The decrease in the barrier height is now down to 8.8 kcal mol^{-1}, 21 kcal mol^{-1} below the threshold of the substrate assisted pathway and 13 kcal mol^{-1} below that of the solvent assisted mechanism. This stabilization of the transition state could be explained because of the stabilizing hydrogen bond interactions between the H atoms of the O bridge and the O atom in para to the $-NO_2$ in the NPP species. Moreover, the product free energies are negative (exergonic), whereas those in Figure 5 are positive (endergonic, solvent-assisted mechanism) or thermoneutral (the substrate-assisted mechanism). Thus, we can affirm that the isomer of $\{Mo_2\}$ dimer in which the O atoms of the bridge are protonated along with the axial O atoms produces a real catalytic effect on the hydrolysis of the phosphoester bond.

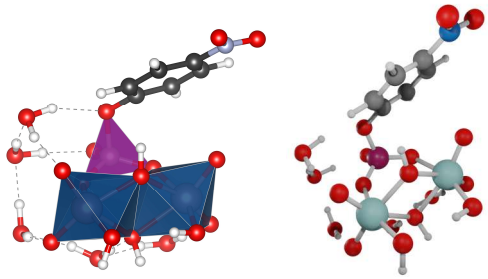

Figure 7. Optimised structure for the dimeric species observed through MS experiments along with the water molecule responsible for the hydrolysis of the substrate.

The $\{Mo_2\}$ species is shown to increase the hydrolysis rate. A quasilinear transition state (OPO ~ 173.6º) was obtained for all the compounds. This highlights the importance of the specific interactions of the water molecules in the mechanism. Not only all the activation energies ($\Delta G^{\ddagger}$) are lower than that obtained for the uncatalyzed reaction but also the hydrolysis of the dimer is somewhat exergonic, whereas for the uncatalyzed reaction it is endergonic for the solvent assisted mechanism, and thermoneutral for the substrate assisted pathway.

Although the transition state associated to the $\{Mo_2\}$ dimeric species with two edge-sharing octahedra capped with equatorial hydroxy groups is 16.4 kcal mol^{-1} lower in energy than that of the non-catalysed substrate assisted mechanism (see Supporting Information), comparing it to the transition state of the non-catalysed solvent assisted pathway this difference is only 8 kcal mol^{-1}.

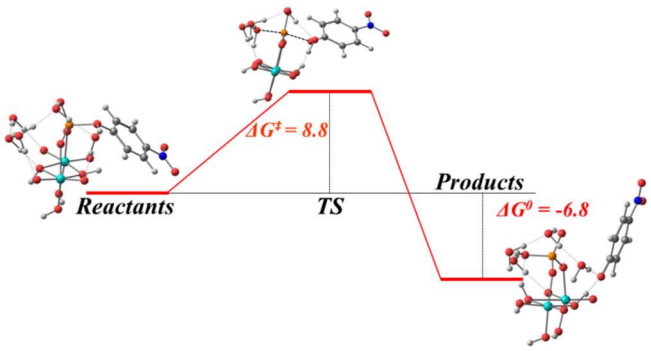

Figure 8. Reaction scheme for *p*NPP hydrolysis activated by the $[Mo_2O_8H_4]^0$ species in which the O bridge atoms are protonated along with the axial O atoms. Four explicit water molecules are considered. Gibbs energies are in kcal mol^{-1}.

The free energy changes of the overall transformations are summarised below:

A) $8H_3O^+ + [Mo_7O_{24}]^{6-} \rightarrow 2[Mo_2O_8H_4] + [Mo_3O_8]^{2+} + 8H_2O$

ΔG^e = -81.3 kcal mol^{-1}

B) $2\,[Mo_2O_8H_4] + [Mo_3O_8]^{2+} + 8\,H_2O \rightarrow [Mo_2O_8H_4] + Mo_5O_{15} + 7\,H_2O + 2\,H_3O^+$

ΔG^e = -79.3 kcal mol^{-1}

C) $8\,H_3O^+ + [Mo_7O_{24}]^{6-} \rightarrow [Mo_2O_8H_4] + Mo_5O_{15} + 7\,H_2O + 2\,H_3O^+$

ΔG^e = -160.6 kcal mol^{-1}

Probing for activity in analogous tungsten species

The same calculations were repeated for tungsten analogues. A comparison of results between both metals is compiled in **Table 2**. The results showed in general higher activation barriers for the same reactions with tungsten analogues. The effect of the addition of explicit water molecules in the calculation was studied for the tungsten dimer as well. Comparative results can be found in the supporting information documents. The results are in agreement with previous studies with Mo systems in which the inclusion of explicit solvent molecules had a relevant effect in reaction barriers of phosphoester hydrolysis. We observe a general decrease in $\Delta G^{\ddagger}$ with the inclusion of additional explicit molecules for both metal dimers. The data are also in agreement with the observations by Parac-Vogt et al. that found no catalytic activity for the tungsten analogue $[W_7O_{24}]^{6-}$, as the activation barriers are higher for $\{W_2\}$ species than for Mo analogues and the general thermodynamic equilibrium is less favourable.

Table 2. Activation and equilibrium free energies ($\Delta G^{\ddagger}$ and ΔG^e/kcal mol^{-1}) of pNPP hydrolysis.

	$\Delta G^{\ddagger}$ / kcal mol^{-1}		ΔG^e / kcal mol^{-1}	
No catalyst substrate assisted	+29.8		+0.6	
No catalyst solvent assisted	+21.4		+16.1	
Species[a]	$\Delta G^{\ddagger}$ Mo / kcal mol^{-1}	$\Delta G^{\ddagger}$ W / kcal mol^{-1}	ΔG^e Mo / kcal mol^{-1}	ΔG^e W / kcal mol^{-1}
$\{Mo_5\}$	+44.1	+44.6	-3.6	-2.0
$\{Mo_2\}$ including 4 explicit H_2O molecules	+8.8	+14.6	-6.8	-1.1

Conclusion

A theory – experiment combined approach was employed in order to elucidate the underlying hydrolysis mechanism of POM-catalyzed DNA-model pNPP. The original work by Parac-Vogt et. al. proposed the activation of the phosphate group by a pentanuclear $\{Mo_5$-pNPP$\}$ precursor. We have shown that this is inconsistent with the results reported in this work. The catalytically active species responsible for the hydrolytic process is most likely to be the dimeric unit $[Mo_2O_4(OH)_4(pNPP)]^{2-}$, which exhibits a lower reaction barrier (+8.8 kcal mol^{-1}) in a more exergonic reaction (-6.8 kcal mol^{-1}) than the uncatalyzed one in marked contrast to the $\{Mo_5\}$ alternative which was shown to have unfavourable free energies. Furthermore, no actual adducts between $\{Mo_5\}$ and pNPP were detected in the ESI-MS spectra. In combination with the obtained computational data, it is likely that the formation equilibrium of $\{Mo_7\}$ with smaller fragments such as $\{Mo_3\}$ and $\{Mo_2\}$ and their subsequent reassembly is the source of the hydrolytic activation rather than a rearrangement of the $\{Mo_5\}$ framework.

Finally, we also studied the analogous pathway for the $\{W_5\}$ and $\{W_2\}$ species and we found that the activation energies for the hydrolytic process are higher than the ones observed for the Mo congeners. The experiments described previously[27] also did not detect any catalytic activity in the presence of the tungsten analogue presumably due to the differing pH window required for the active species to form.

Experimental Section

Computational Details

DFT calculations were performed using the Amsterdam Density Functional 2017.01 (ADF) program package. Geometry optimizations, without symmetry constraints, were performed resorting to a combination of the gradient corrections of Becke 1998 exchange functional and Perdew 1986 correlation functional as well as the latest version of Grimme dispersion correction (BP86-D3). Relativistic effects were treated with the Zero Order Regular Approximation (ZORA) Hamiltonian. The frozen core approximation was employed, thus, triple-ζ Slater-type orbitals (STO) were used to describe the valence shells of C and N (2s and 2p). One polarization function was added to C, N, O, Mo and W (single-ζ, 3d, 4f). Triple-ζ STOs were used to describe the valence shells of H (1s) augmented with one polarization function (single-ζ, 2s, 2p). Solvent effects were treated with the Conductor-like Screening Model (COSMO) of solvation (Water, ε=78.39). Analytical frequencies were calculated to characterise the obtained stationary points and calculate the free energies (standard state T=298.15K, P= 1atm). Transition states were followed after a fractional displacement of the imaginary vibrational mode to both the reactant(s) and product(s). The starting structures were modelled after the reported $[Mo_7O_{24}]^{6-}$ and $[Mo_5O_{15}(pNPP)_2]^{4-}$ geometries. Molecular renderings were made with VESTA[66] and Chemcraft[67] Optimised structures were deposited in the iochem-bd database[68] and may be visualised at the following link https://dx.doi.org/10.19061/iochem-bd-6-70.

ESI experimental

All MS data were collected using a Q-trap, time-of-flight MS (Maxis Impact MS) instrument supplied by Bruker Daltonics Ltd. The detector was a time-of-flight, micro-channel plate detector and all data was processed using the Bruker Daltonics Data Analysis 4.1 software, whilst simulated isotope patterns were investigated using Bruker Isotope Pattern software and Molecular Weight Calculator 6.45. The calibration solution used was Agilent ES tuning mix solution, Recorder No. G2421A, enabling calibration between approximately 100 *m/z* and 3000 *m/z*. This solution was diluted 60:1 with MeCN. Samples were dissolved in MeOH and introduced into the MS *via* direct injection at 180 μL h^{-1}. The ion polarity for all MS scans recorded was negative, at 180 °C, with the voltage of the capillary tip set at 4000 V, end plate offset at –500 V, funnel 1 RF at 300 Vpp and funnel 2 RF at 400 Vpp.

Acknowledgements

This research was financially supported by the Fundação para a Ciência e a Tecnologia (FCT) by means of the project PTDC/QUI-QFI/29236/2017, UID/MULTI/00612/2019, UID/MULTI/04046/2019,

UIDB/04046/2020, UIDP/04046/2020 and by the Spanish Ministry of Economy, Industry and Competitiveness under the Maria de Maeztu Units of Excellence Programme – MDM-2016-0618. A.G. is thankful to Diputación Foral de Gipuzkoa for current funding in the frame of Gipuzkoa Fellows Program. HNM thanks the University of Glasgow. Dr Ángel Sánchez is grateful to Prof. Francisco Fernandez for fruitful discussions. This research was also funded by Eusko Jaurlaritza (the Basque Government), through Consolidated Group Project No. IT1254-19, and the Spanish MINECO/FEDER Project No. PGC2018-097529-B-100. Technical and human support provided by IZO-SGI, SGIker (UPV/EHU, MICINN, GV/EJ, ERDF and ESF) is gratefully acknowledged.

Keywords: polyoxometalate • phosphoester hydrolysis • DFT • DNA • Artificial phophoesterases

[1] P. Gouzerh and M. Che, *L'Act. Chim.* **2006**, *298*, 9-22.
[2] N. N. Greenwood and A. Earnshaw in *Chemistry of the Elements* (2nd ed.), Oxford: Butterworth-Heinemann, **1997**.
[3] P. Miró, S. Pierrefixe, M. Gicquel, A. Gil, C. Bo, *J. Am. Chem. Soc.* **2010**, *132*, 17787-17794.
[4] A. Gil, D. Karhánek, P Miró, M. R. Antonio, M. Nyman, C. Bo, *Chem. Eur. J.* **2012**, *18*, 8340-8346.
[5] E. Tiferet, A. Gil, C. Bo, T. Y. Shvareva, M. Nyman, A. Navrotsky, *Chem. Eur. J.* **2014**, *20*, 3646-3651.
[6] P. Miró, B. Vlaisavljevich, A. Gil, P. C. Burns, M. Nyman, C. Bo, *Chem. Eur. J.* **2016**, *22*, 8571-8578.
[7] P. Yang, T. Ma, Z. Lang, S. Misirlic-Dencic, A. M. Isakovic, A. Bénvei, M. B. Čolović, I. Markovic, D. Z. Krstić, J. M. Poblet, Z. Lin, U. Kortz, *Inorg. Chem.* **2019**, *58*, 11294-11299.
[8] W. W. Ayass, T. Fodor, Z. Lin, R. M. Smith, X. Xing, K. Abdallah, I. Tóth, L. Zékány, M. Pascual-Borràs, A. Rodríguez-fortea, J. M. Poblet, L. Fan, J. Cao, B. Keita, M. S. Ulrich, U. Kortz, *Inorg. Chem.* **2016**, *55*, 10118-10121.
[9] A. Hiskia, A. Troupis, S. Antonaraki, E. Gkika, P. Kormali, E. Papaconstantinou, *Int. J. Env. Anal. Chem.* **2006**, *86*, 233-242.
[10] C. Busche, L. Vilà-Nadal, J. Yan, H. N. Miras, D. L. Long, V. P. Georgiev, A. Asenov, R. H. Pedersen, N. Gadegaard, M. M. Mirza, D. J. Paul, J. M. Poblet, L. Cronin, *Nature* **2014**, *515*, 545-549.
[11] J. Lehmann, A. Gaita-Ariño, E. Coronado, D. Loss, *Nanotechnology* **2007**, *2*, 312-317.
[12] H. I. Buvailo, V. G. Makhankova, V. N. Kokozay, I. V. Omelchenko, S. V. Shishkina, J. Jezierska, M. V. Pavliuk, S. I. Shylin, *Inorg. Chem. Front.* **2019**, *6*, 1813-1823.
[13] J. T. Rhule, C. L. Hill, D. A. Judd, R. F. Schinazi, *Chem. Rev.* **1998**, *98*, 327-358.
[14] B. Hasenknopt, *Front Biosci.* **2005**, *10*, 275-287.
[15] Y. Toshihiro in *Polyoxometalates for Molecular Devices: Antitumor Activity and Luminescence* (Eds.: M. Pope and A. Müller) Polyoxometalates: From Platonic Solids to Anti-Retroviral Activity – Springer **1994**, pp. 337-358.
[16] X. Wang, J. Liu, J. Li, Y. Yang, J. Liu, B. Li, M. T. Pope, *J. Inorg. Biochem.* **2003**, *94*, 279-284.
[17] J. Li, Y. Qi, J. Li, H. Wang, X. Wu, L. Duan, E. Wang, *J. Coord. Chem.* **2004**, *57*, 1309-1319.
[18] H. U. Gerth, A. Rompel, B. Krebs, J. Boos, C. Lanvers-Kaminsky, *Anti-Cancer Drugs* **2005**, *16*, 101-106.
[19] X. Wang, F. Li, S. Liu, M. T. Pope, *J. Inorg. Biochem.* **2005**, *99*, 452-457.
[20] A. Ogata, S. Mitsui, H. Yanagie, H. Kasano, T. Hisa, T. Yamase, M. Eriguchi, *Biomed. Parmacother.* **2005**, *59*, 240-244.
[21] A. Bijelic, M. Aureliano, A. Rompel, *Angew. Chem. Int. Ed.* **2018**, *58*, 2980-2999.
[22] A. Bijelic, M. Aureliano, A. Rompel, *Chem. Commun.* **2018**, *54*, 1153-1169.
[23] T. Ma, P. Yang, I. Damman, Z. Lin, A. S. Mougharbel, M.-X. Li, F. Adăscălitei, R. Mitea, C. Silvestru, C. Thorstenson, M. S. Ulrich, K. Cseh, M. A. Jakupec, B. K. Keppler, M. Donalisio, R. Cavalli, D. Lembo, U. Kortz, *Inorg. Chem.* **2020**, *59*, 2978-2987.
[24] A. Radzicka and R. Wolfenden, *Science* **1995**, *267*, 90-93.
[25] C. M. Tomé, M. C. Oliveira, M. Pillinger, I. S. Gonçalves, M. Abrantes, *Dalton Trans.* **2013**, *42*, 3901-3907.
[26] B. Alberts *in Molecular Biology of the Cell* (6 ed.) Garland Science **2017**.
[27] E. Cartuyvels, G. Absillis, T. N. Parac-Vogt, *Chem. Commun.* **2008**, *1*, 85-87.
[28] L. Van Lokeren, E. Cartuyvels, G. Absillis, R. Willem, T. N. Parac-Vogt, *Chem. Commun.* **2008**, *24*, 2774-2776.
[29] E. Cartuyvels, K. Van Hecke, L. Van Meervelt, C. Goerller-Walrand, T. N. Parac-Vogt, *Inorg. Biochem.* **2008**, *102*, 1589-1598.
[30] G. Absillis, E. Cartuyvels, R. Van Deun, T. N. Parac-Vogt, *J. Am. Chem. Soc.* **2008**, *130*, 17400-17408.
[31] G. Absillis, R. Van Deun, T. N. Parac- Vogt, *Inorg. Chem.* **2011**, 50, 11552-11560.
[32] S. Vanhaecht, G. Absillis, T. N. Parac-Vogt, *Dalton Trans.* **2012**, *41*, 10028-10034.
[33] W. Li, T. Rudack, K. Gerwert, F. Gräter, J. Schlitter, *J. Chem. Theory Comput.* **2012**, *8*, 3596-3604.
[34] P. Nunes, A. C. Gomes, M. Pillinger, I. S. Gonçalves, M. Abrantes, *Micropor. Mesopor. Mat.* **2015**, *208*, 21-29.
[35] A. C. Gomes, C. A. Gamelas, J. A. Fernandes, F. A. Almeida, P. Nunes, M. Pillinger, I. S. Gonçalves, C. C. Romão, M. Abrantes, *Eur. J. Inorg. Chem.* **2014**, *2014*, 3681-3689.
[36] A. C. Gomes, M. Pillinger, P. Nunes, I. S. Gonçalves, M. Abrantes, *J. Organomet. Chem.* **2014**, *760*, 42-47.
[37] L. Lain, H. Lönnberg, T. Lönnberg, *Chem. Eur. J.* **2013**, *19*, 12424-12434.
[38] P. Das, N. B. Chandar, S. Chourey, H. Agarwalla, B. Ganguly, A. Das, *Inorg. Chem.* **2013**, *52*, 11034-11041.
[39] T. K. N. Luong, G. Absillis, P. Shestakova, T. N. Parac-Vogt, *Eur. J. Inorg. Chem.* **2014**, *2014*, 5276-5284.
[40] T. K. N. Luong, G. Absillis, P. Shestakova, T. N. Parac-Vogt, *Dalton Trans.* **2015**, *44*, 15690-15696.
[41] T. K. N. Luong, P. Shestakova, T. T. Mihaylov, G. Absillis, K. Pierloot, T. N. Parac-Vogt, *Chem. Eur. J.* **2015**, *21*, 4428-4439.
[42] E. Gouré, M. Carboni, A. Troussier, C. Lebrun, J. Pécaut, J. F. Jacquot, P. Dubourdeaux, M. Clémancey, G. Blondin, J. M. Latour, *Chem. Eur. J.* **2015**, *21*, 8064-8068.
[43] T. K. N. Luong, P. Shestakova, T. N. Parac-Vogt, *Dalton Trans.* **2016**, *45*, 12174-12180.
[44] S. Bosch, P. Comba, L. R. Gahan, G. Schenk, *J. Inorg. Biochem.* **2016**, *162*, 343-355.
[45] B. Kandasamy, S. Vanhaecht, F. M. Nkala, T. Beelen, B. S. Bassil, T. N. Parac-Vogt, U. Kortz, *Inorg. Chem.* **2016**, *55*, 9204-9211.
[46] T. K. N. Luong, T. T. Mihaylov, G. Absillis, P. Shestakova, K. Pierloot, T. N. Parac-Vogt, *Inorg. Chem.* **2016**, *55*, 9898-9911.
[47] T. K. N. Luong, I. Govaerts, J. Robben, P. Shestakova, T. N. Parac-Vogt, *Chem. Commun.* **2017**, *53*, 617-620.
[48] A. De, S. Pradhan, S. Sitangshu, B. Biswas, *J. Indian Chem. Soc,* **2017**, *94*, 1063-1071.
[49] X.-L. Huang, *Astrobiology* **2018**, *18*, 294-310.
[50] Q. Hu, V. M. Jayasinghe-Arachchige, J. Zuchniarz, R. Prabhakar, *Front.Chem.* **2019**, *7*, 195.
[51] H. Kou, Y. Wang, P. Ding, J. Li, B. Shi, *J. Coord. Chem.* **2019**, *72*, 1683-1696.
[52] C. Pereira, G. Farias, F. G. Maranha, N. Castilho, G. Schenk, B. de Souza, H. Terenzi, A. Neves, R. A. Peralta, *J. Biol. Inorg.* **2019**, *24*, 675-691.
[53] Q. Hu, V. M. Jayasinghe-Arachchige, G. Sharma, L. F. Serafim, T. J. Paul, R. Prabhakar, *Wiley Interdiscip. Rev. Comput. Mol. Sci.* **2020**, DOI: https://doi.org/10.1002/wcms.1466
[54] J. R. Morrow and W. C. Trogler, *Inorg. Chem.* **1988**, *27*, 3387-3394.
[55] T. Koike and E. Kimura, *J. Am. Chem. Soc.* **1991**, *113*, 8935-8941.
[56] S. Amin, D. A. Voss Jr., W. D. Horrocks Jr., J. R. Morrow, *Inorg. Chem.* **1996**, *35*, 7466-7467.
[57] S. Amin, D. A. Voss Jr., W. D. Horrocks Jr., C. H. Lake, M. R. Churchill, J. R. Morrow, *Inorg. Chem.* **1995**, *34*, 3294-3300.
[58] K. O. A. Chin, J. R. Morrow, *Inorg. Chem.* **1994**, *33*, 5036-5041.
[59] H. N. Miras, D. Stone, D. L. Long, E. J. L. McInnes, P. Kögerler, L. Cronin, *Inorg. Chem.* **2011**, *50*, 8384-8391.
[60] E. F. Wilson, H. N. Miras, M. H. Rosnes, L. Cronin, *Angew. Chem. – Int. Ed.* **2011**, *50*, 3720-3724.
[61] H. Zang, A. Surman, D. Long, L. Cronin, H. N. Miras, *Chem. Commun.* **2016**, *52*, 9109-9112.
[62] H. Y. Zang, J. J. Chen, D. L. Long, L. Cronin, H. N. Miras, *Adv. Mater.* **2013**, *25*, 6245-6249.

[63] L. Pettersson, I. Andersson, L.-O.Öhman, *Inorg. Chem.* **1986**, *25*, 4726-4733.
[64] J. Fischer, L. Ricard, P. Toledano, *J. Chem. Soc. Dalton Trans.* **1974**, 941-946.
[65] F. Duarte, J. Åqvist, N. H. Williams, S. C. L. Kamerlin, *J. Am. Chem. Soc.* **2015**, *137*, 1081-1093.
[66] K. Momma, F. Izumi, *J. Appl. Crystallogr.* **2011**, *44*, 1272-1276.
[67] http://www.chemcraftprog.com.
[68] M. Álvarez-Moreno, C. de Graaf, N. López, F. Maseras, J. M. Poblet, C. Bo, *J. Chem. Inf. Model.* **2015**, 55, 95-103.